


Review

Continuous-Wave Self-Raman Vanadate Lasers Generating Versatile Visible Wavelengths

Di Li ¹, Chien-Yen Huang ¹, Xiu-Wei Chang ¹, Hsing-Chih Liang ² and Yung-Fu Chen ^{1,*} 

¹ Department of Electrophysics, National Yang Ming Chiao Tung University, Hsinchu 30010, Taiwan; dili.sc09@nycu.edu.tw (D.L.); so3355589.sc09@nycu.edu.tw (C.-Y.H.); xiaoxiu.sc11@nycu.edu.tw (X.-W.C.)

² Institute of Physics, National Yang Ming Chiao Tung University, Hsinchu 30010, Taiwan; hcliang@nycu.edu.tw

* Correspondence: yfchen@nycu.edu.tw

Abstract: In this review, the developments of efficient high-power CW orange-lime-green lasers by using intracavity stimulated Raman Scattering (SRS) in Nd-doped vanadate lasers are systematically discussed. The overall properties of the spontaneous Raman spectra in Nd:YVO₄ and Nd:GdVO₄ crystals are overviewed. The critical phase matchings of using the lithium triborate (LBO) crystals for sum frequency generation (SFG) and second harmonic generation (SHG) are thoroughly reviewed. We make a detailed review for achieving the individual green-lime-orange emissions from the self-Raman Nd:YVO₄ and Nd:GdVO₄ lasers with LBO crystals. The following is to review the dual-wavelength operations of the lime-green and orange-green lasers. Finally, the procedure for generating the triple-wavelength operation of orange-lime-green simultaneous emissions is completely described. The present review is expected to be useful for developing compact, efficient, high-power CW visible lasers for applications including medical treatment, biology, spectroscopy, and remote sensing.

Keywords: stimulated Raman scattering; visible lasers; self-Raman; vanadate crystal; LBO



Citation: Li, D.; Huang, C.-Y.; Chang, X.-W.; Liang, H.-C.; Chen, Y.-F. Continuous-Wave Self-Raman Vanadate Lasers Generating Versatile Visible Wavelengths. *Photonics* **2024**, *11*, 601. <https://doi.org/10.3390/photonics11070601>

Received: 5 June 2024

Revised: 19 June 2024

Accepted: 25 June 2024

Published: 26 June 2024



Copyright: © 2024 by the authors. Licensee MDPI, Basel, Switzerland. This article is an open access article distributed under the terms and conditions of the Creative Commons Attribution (CC BY) license (<https://creativecommons.org/licenses/by/4.0/>).

1. Introduction

Intracavity second harmonic generation (SHG) of the fundamental field in neodymium (Nd) doped lasers is the most used method to generate high-power continuous-wave (CW) green lasers. In addition to the green laser, there is a growing demand for multi-watt CW lime-yellow laser sources for retinal photocoagulation, especially in the treatment of macula. This demand comes from the fact that the macula contains abundant xanthophyll pigments that have a small amount of absorption for green light and almost no absorption in the lime-yellow spectral region. Since the treatment laser absorbed by xanthophyll pigments may cause collateral damage to the eye, high-power lime-yellow light sources become requisite for retinal photocoagulation near the macula [1–4].

Stimulated Raman scattering (SRS) is a practical and useful approach to widen the wavelength range from ultraviolet to mid-infrared. The SRS phenomenon was originally observed by Woodbury and Ng in 1962 from the exploration of Q-switched ruby lasers with nitrobenzene materials [5]. Nowadays, intracavity SRS by using solid-state crystals is an efficient and reliable method to extend the spectral range of solid-state lasers [6–10]. Nd-doped solid-state lasers have been successfully demonstrated to realize compact high-power CW lime-yellow-orange light sources by combining intracavity SRS in a Raman gain medium with sum frequency generation (SFG) or SHG in a nonlinear crystal [11–16].

Nowadays, the most popular gain media for intracavity SRS are tungstate crystals [17–35] such as BaWO₄, SrWO₄, KGd(WO₄)₂, and vanadate crystals such as GdVO₄ [36–48], YVO₄ [49–91], and LuVO₄ [92,93]. In particular, the Nd-doped vanadate laser materials are often categorized as self-Raman materials since they can simultaneously generate the fundamental laser field and the Raman Stokes field. Using the V-O stretching mode of Nd:GdVO₄ crystal with the Raman frequency shift of 882 cm^{−1}, the wavelength of the

Stokes field is approximately 1173 nm for the 1063-nm fundamental field. Consequently, the SHG of the Stokes field and the SFG of the Stokes field with the fundamental field can yield the lasers at 586 nm (orange) and 558 nm (lime), respectively. On the other hand, the wavelength of the Stokes field in the Nd:YVO₄ crystal is around 1176 nm for the 1064-nm fundamental field with the Raman frequency shift of 890 cm⁻¹. Therefore, the lime and orange wavelengths generated using the Nd:YVO₄ crystal are 559 nm and 588 nm, respectively. So far, both Nd:GdVO₄ [41–45] and Nd:YVO₄ [86–89] crystals have been widely used to generate multi-watt CW lime and orange lasers. The linear resonator is usually used to achieve the criterion of ultralow losses for efficiency in the CW intracavity SRS process. Since Nd-doped vanadate materials possess a high absorption in the green-lime-orange wavelengths, an intracavity dichroic coating was often exploited in the two-mirror linear resonator to reflect the backward SHG/SFG for eliminating the absorption [86–89].

In this review, we make a thorough discussion of the recent development of efficient high-power CW orange-lime-green lasers based on intracavity SRS in Nd-doped vanadate lasers with SFG and SHG in lithium triborate (LBO) crystals. In Section 2, the characterizations of the spontaneous Raman spectra in Nd:YVO₄ and Nd:GdVO₄ crystals are completely reviewed. In Section 3, the critical phase matchings of LBO crystal for visible emissions from SFG and SHG are discussed. In Section 4, we review the results of single wavelength operations for individual green-lime-orange emissions [86]. Then, the dual-wavelength operations of the lime-green [87] and orange-green [88] lasers are completely reviewed in Section 5. Finally, we review the results for the triple-wavelength operation of orange-lime-green simultaneous emissions [89]. It is believed that the present review for compact, efficient, high-power CW visible lasers will be of practical usefulness for applications such as medical treatment, biology, spectroscopy, and remote sensing. In addition to CW operation, an effective and reliable method for developing dual-wavelength passive Q-switched self-Raman lasers with controllable polarization has also progressed recently [49].

2. Spontaneous Raman Spectrum of Vanadate Crystals

First of all, the spontaneous Raman spectra of vanadate crystals are briefly reviewed. The configuration of the Raman scattering measurement is usually indicated by the Porto notation [94] that specifies the orientation of the crystal with respect to the polarization of the laser in both the excitation and analyzing directions for Raman scattering processes. The Porto notation consists of four letters: A(BC)D, where A is the direction of the propagation of the incident light (\mathbf{k}_i), B is the direction of the polarization of the incident light (\mathbf{E}_i), C is the direction of the polarization of the scattered light (\mathbf{E}_s), and D is the direction of the propagation of the scattered light (\mathbf{k}_s).

Figure 1a,b shows the experimental data of the spontaneous Raman scattering spectra of YVO₄ crystal with the Porto notations of X(ZZ) \bar{X} and X(YY) \bar{X} . Both Raman configurations in the YVO₄ crystal can be observed to have different active vibration modes. Furthermore, the spectra reveal several conspicuous Raman peaks associated with the internal modes of the VO₄³⁻ group as well as the external modes of VO₄³⁻ tetrahedra and Y³⁺ ions in the YVO₄ unit cell. The external mode at 157 cm⁻¹ (B_{1g}(1)), related to the O–Y–O bending vibration, can be found in both Raman configurations. Additionally, the internal modes, which can be attributed to the VO₄ bending and stretching vibrations, situated at higher wave numbers: 259 (B_{2g}), 376 (A_{1g}(1)), 487 (B_{1g}(3)), 816 (B_{1g}(4)), 838 (E_g(5)), and 890 cm⁻¹ (A_{1g}(2)) can be entirely observed in the X(YY) \bar{X} configuration. However, the vibrations at 487 and 816 cm⁻¹ are not found in the X(ZZ) \bar{X} configuration. The strongest vibrational Raman peak can be confirmed to be located at 890 cm⁻¹ with a Raman line width of 3.0 cm⁻¹. The Raman gain coefficient was estimated to be approximately 5 cm/GW [95]. The Raman gain coefficients of two weak Raman shifts, 838 and 376 cm⁻¹, in the X(ZZ) \bar{X} configuration are estimated to be 1.3 and 2.0 cm/GW, respectively. On the other hand, the Raman gain coefficients of two weak Raman shifts, 838 and 816 cm⁻¹, in the X(YY) \bar{X} configuration are estimated to be 2.5 and 1.5 cm/GW, respectively. Figure 2a,b shows the

experimental data of the spontaneous Raman scattering spectra of GdVO₄ crystal with the Porto notations of X(ZZ) \bar{X} and X(YY) \bar{X} . The overall characteristics of the spontaneous Raman scattering spectra can be clearly seen to be similar to the results shown in Figure 1 for the YVO₄ crystal.

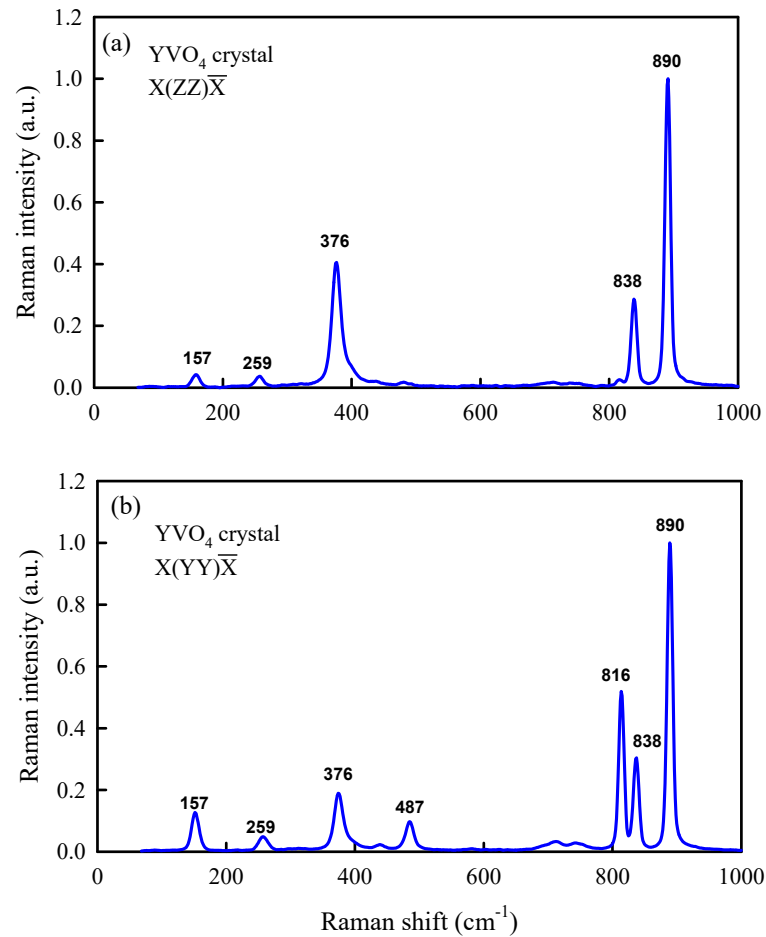


Figure 1. Experimental data of the spontaneous Raman scattering spectra of YVO₄ crystal with the Porto notations of (a): X(ZZ) \bar{X} and (b): X(YY) \bar{X} .

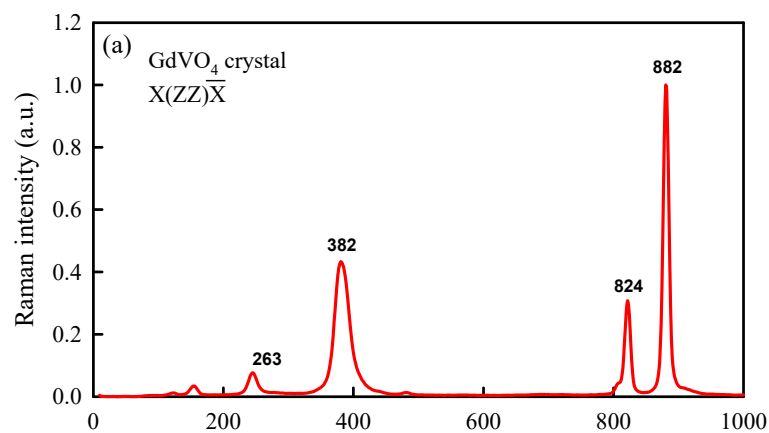


Figure 2. Cont.

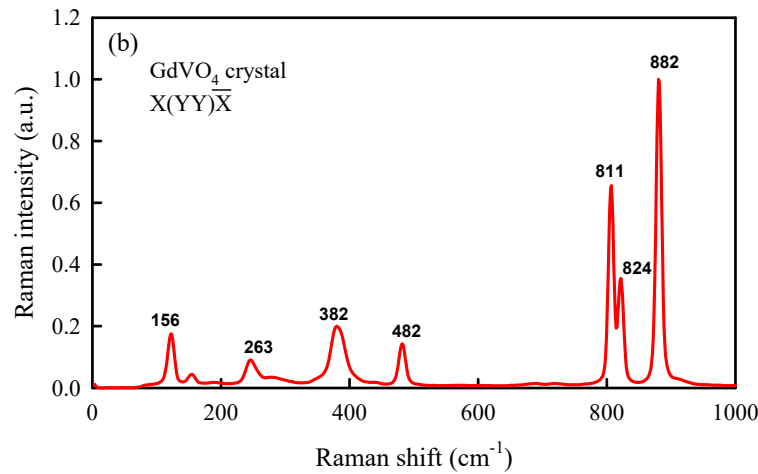


Figure 2. Experimental data of the spontaneous Raman scattering spectra of GdVO₄ crystal with the Porto notations of (a): X(ZZ) \bar{X} and (b): X(YY) \bar{X} .

3. The Critical Phase Matching of LBO Crystal for Visible Emissions

The LBO crystal [96], belonging to an orthorhombic system with point group symmetry of mm², is the most widely used nonlinear material for generating visible lights from SHG and SFG of self-Raman vanadate lasers. The high-quality growth and the nonlinear characterizations of the LBO crystal were originally and mainly explored by the Fujian Institute of Research on the Structure of Matter, Chinese Academy of Sciences. The LBO material is a negative biaxial crystal with a high damage threshold that makes it superior in the high-power SHG and SFG. Moreover, the LBO crystal can achieve high conversion efficiencies for a wide-ranging spectrum.

The unit cell dimensions of the LBO crystal are given by a = 8.4473 Å, b = 7.3788 Å, c = 5.1395 Å. The crystallographic axes a, c, and b are one-to-one parallel to the principal axes X, Y, and Z ($n_z > n_y > n_x$). For the LBO crystal, the Sellmeier equations of n_x , n_y , and n_z with the temperature dependence can be expressed as [96]

$$n_x(\lambda, T) = \left(2.4542 + \frac{0.01125}{\lambda^2 - 0.01135} - 0.01388\lambda^2 \right)^{1/2} + \frac{dn_x}{dT}(T - T_0), \quad (1)$$

$$n_y(\lambda, T) = \left(2.5390 + \frac{0.01277}{\lambda^2 - 0.01189} - 0.01848\lambda^2 \right)^{1/2} + \frac{dn_y}{dT}(T - T_0), \quad (2)$$

$$n_z(\lambda, T) = \left(2.5865 + \frac{0.01310}{\lambda^2 - 0.01223} - 0.01861\lambda^2 \right)^{1/2} + \frac{dn_z}{dT}(T - T_0), \quad (3)$$

where λ is the wavelength with the units of micrometer, T is the temperature with the units of degrees Celsius, and $T_0 = 20$ °C. Velsko et al. [97] earlier published the thermo-optical coefficients that were simply expressed as

$$\frac{dn_x}{dT} = -1.8 \times 10^{-6}, \quad (4)$$

$$\frac{dn_y}{dT} = -13.6 \times 10^{-6}, \quad (5)$$

$$\frac{dn_z}{dT} = -(6.3 + 2.1\lambda) \times 10^{-6}. \quad (6)$$

Tang et al. [98] later studied the temperature-dependent thermo-optical coefficients and modified them as

$$\frac{dn_x}{dT} = 2.0342 \times 10^{-7} - 1.9697 \times 10^{-8}T - 1.4415 \times 10^{-11}T^2, \quad (7)$$

$$\frac{dn_y}{dT} = -1.0748 \times 10^{-5} - 7.1034 \times 10^{-8}T - 5.7387 \times 10^{-11}T^2, \quad (8)$$

$$\frac{dn_z}{dT} = -8.5998 \times 10^{-7} - 1.5476 \times 10^{-7}T + 9.4675 \times 10^{-10}T^2 - 2.2375 \times 10^{-12}T^3. \quad (9)$$

The type-I phase matching in the XY plane of the LBO crystal is similar to that in the negative uniaxial crystal. The condition for the phase matching of SFG can be expressed as

$$\frac{n_z(\lambda_1, T)}{\lambda_1} + \frac{n_z(\lambda_2, T)}{\lambda_2} = \frac{n_{xy}^e(\lambda_3, T, \phi)}{\lambda_3}, \quad (10)$$

where $\lambda_1^{-1} + \lambda_2^{-1} = \lambda_3^{-1}$ and the effective refractive index $n_{xy}^e(\lambda, T, \phi)$ is given by

$$n_{xy}^e(\lambda, T, \phi) = \left[\frac{\sin^2 \phi}{n_x^2(\lambda, T)} + \frac{\cos^2 \phi}{n_y^2(\lambda, T)} \right]^{-1/2}, \quad (11)$$

From Equation (10), the condition of the phase matching can be manifested by using the function of the wave number difference given by [96]

$$\Delta k = \frac{n_z(\lambda_1, T)}{\lambda_1} + \frac{n_z(\lambda_2, T)}{\lambda_2} - \frac{n_{xy}^e(\lambda_3, T, \phi)}{\lambda_3}, \quad (12)$$

For attaining high conversion efficiency, the phase-matching condition $\Delta k = 0$ needs to be satisfied. In the self-Raman Nd:YVO₄ laser cavity, the fundamental wavelength at 1064 nm and the Stokes wavelength at 1176 nm can be used for the green (532 nm), lime (559 nm), and orange (588 nm) lasers from the SHG of 1064 nm, the SFG of 1064 and 1176 nm, and the SHG of 1176 nm, respectively. One way to satisfy the phase-matching condition is to employ a non-critically phase-matched (NCPM, $\theta = 90^\circ$, $\phi = 0^\circ$) LBO crystal with tuning the crystal temperature [41–45]. Alternatively, the green (532 nm), lime (559 nm), and orange (588 nm) lasers can be selectively generated by exploiting the different LBO crystals with different cutting angles to reach the type-I phase-matching at room temperature of 25 °C. Figure 3 shows the numerical calculations for the phase-matching condition Δk as a function of the cut angle for the LBO crystal in the XY plane for generating 532, 559, and 588 nm from the fundamental and Stokes waves of 1064 and 1176 nm at room temperature. The optimal cut angles for generating the wavelengths of 532, 559, and 588 nm can be found to be approximately $\phi = 11.6^\circ$, 8.1° , and 4.1° , respectively. As usual, the length of the LBO crystal used in the self-Raman lasers was 8 mm long with anti-reflection coating on both end surfaces at wavelengths of the fundamental and Stokes waves as well as the green-lime-orange outputs.

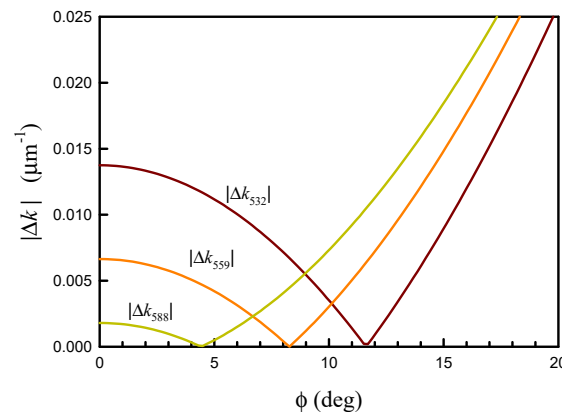


Figure 3. Numerical calculations for the phase-matching condition Δk as a function of the cut angle for the LBO crystal in the XY plane for generating 532, 559, and 588 nm from the fundamental and Stokes waves of 1064 and 1176 nm at room temperature.

4. Single Wavelength Operations for Individual Green-Lime-Orange Emissions

Here, we review employing the self-Raman crystal in the same two-mirror linear cavity to generate three wavelengths for the green, lime, and orange lasers by using three different LBO crystals for intracavity SHG or SFG with the critical phase matching near room temperature [86]. Figure 4 depicts the cavity configuration for generating high-power CW Nd:YVO₄ (Nd:GdVO₄) visible lasers at three different wavelengths of 532 (531.5), 559 (558), and 588 (586) nm. Two kinds of laser crystals, *a*-cut Nd:GdVO₄ and Nd:YVO₄, were individually employed to play the dual roles of lasing and SRS gain medium. A detailed comparison of the output efficiency between Nd:YVO₄ and Nd:GdVO₄ crystals was systematically performed. For both gain media, the Nd³⁺ dopant concentrations and the crystal sizes were the same, 0.3-at.% and 3 × 3 × 20 mm³, respectively. Although the effective crystal length for the laser crystal to absorb the pump power at 808 nm was only approximately 8 mm, a length of up to 20 mm was exploited to enhance the gain of SRS. The surface of the laser crystal toward the input mirror had an anti-reflection coating at 808 and 1060–1190 nm (reflectance < 0.2%). The other surface had a dichroic coating, the measured reflectance of which is shown in Figure 5. For both gain media, the reflectance can be seen to be generally higher than 97% in the range of 530–590 nm. Furthermore, the values of the reflectance at the wavelengths around 1064 nm and 1176 nm are as low as 0.11% and 0.28%, respectively. In the experiment, the laser materials were covered with indium foil and mounted in a copper holder with active conduction cooling at a temperature of 20 °C.

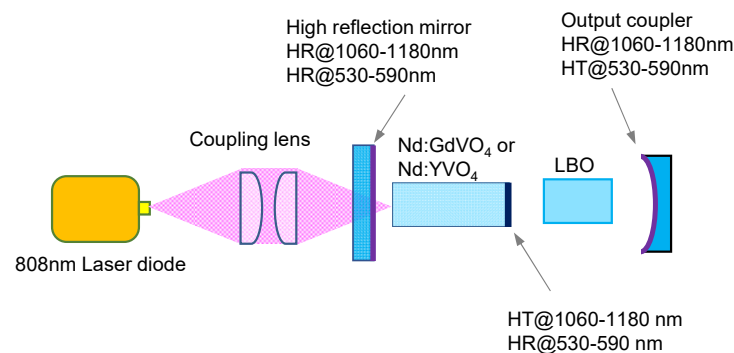


Figure 4. Cavity configuration for generating high-power CW Nd:YVO₄ (Nd:GdVO₄) visible lasers at three different wavelengths of 532 (531.5), 559 (558), and 588 (586) nm.

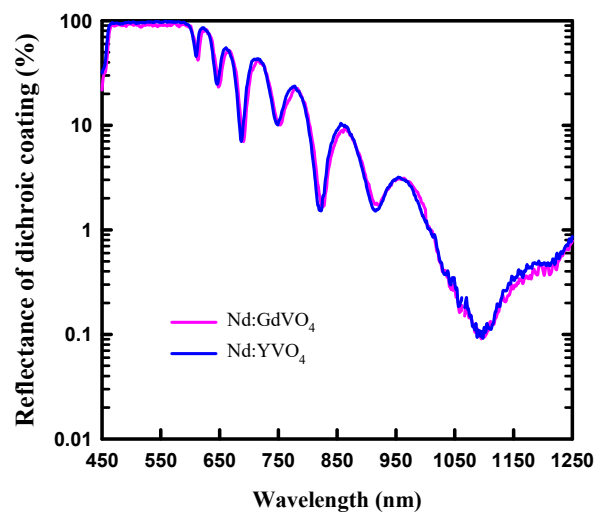


Figure 5. Measured reflectance of the surface coating of the laser crystal toward the input mirror.

The excitation light was a fiber-coupled laser diode that had a central wavelength of 808 nm, core diameter of 600 μm , and numerical aperture of 0.16. The pump source was focused into the laser crystal with a waist radius of approximately 300 μm . The entrance face of the input flat mirror had an anti-reflection coating at 808 nm (reflectance < 0.2%), and the second surface had a high-reflection coating at 1060–1180 nm (reflectance > 99.9%) and a high-transmission coating at 808 nm (transmittance > 95%). The concave output coupler with a radius of curvature of 100 mm had a high-reflection coating at 1060–1180 nm (reflectance > 99.9%) and a high-transmission coating (transmittance > 95%) at 530–590 nm on the concave surface and an anti-reflection coating at 530–590 nm (reflectance < 0.2%) on the other surface. By using three LBO crystals with different cutting angles for the type-I phase-matching, the green, lime, and orange lasers can be individually generated from the same cavity mirrors and gain medium. A thermo-electric cooler was utilized to tune the temperatures of the LBO crystal for optimal operation. The overall cavity length was around 50 mm.

When an 8-mm-long LBO material with the cutting angle at $\theta = 90^\circ$ and $\phi = 4.1^\circ$ was used in the cavity, the orange laser could be generated via the SHG of the Raman Stokes field. Figure 6 shows the average output powers versus the incident pump power for 586 and 588 nm obtained with the Nd:GdVO₄ and Nd:YVO₄ crystals, respectively. The lasing thresholds for 586 and 588 nm outputs are just the thresholds for the SRS process and can be seen to be approximately 3.3 and 4.3 W, respectively. Since the sole difference between these two performances lies in the laser crystal, the overall Raman gain of the GdVO₄ crystal can be, therefore, deduced to be approximately 1.3 times higher than that of the YVO₄ crystal. Due to the higher Raman gain, the output power of 3.4 W generated from the Nd:GdVO₄ crystal is evidently greater than 2.6 W from the Nd:YVO₄ crystal at a pump power of 26 W. The beam quality factors for the overall outputs were found to be around 3.5–4.0.

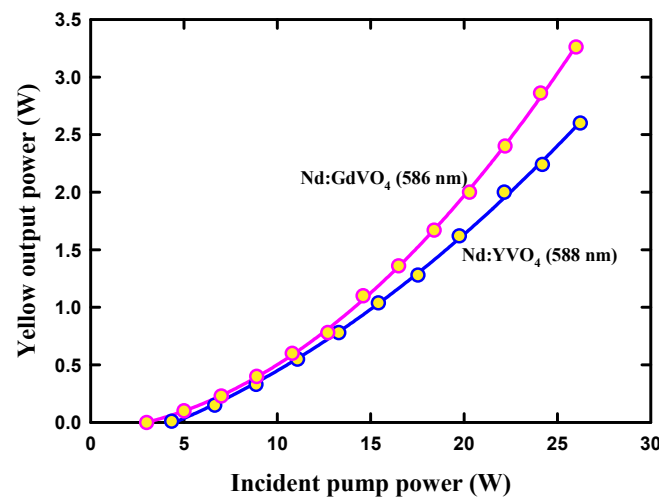


Figure 6. Average output powers versus the incident pump power for 586 and 588 nm obtained with the Nd:GdVO₄ and Nd:YVO₄ crystals, respectively.

When an 8-mm-long LBO material with the cutting angle at $\theta = 90^\circ$ and $\phi = 8.1^\circ$ was employed in the cavity, the lime laser could be generated through the SFG of the fundamental wave and Raman Stokes field. Figure 7 shows the average output powers versus the incident pump power for 558 and 559 nm generated from the Nd:GdVO₄ and Nd:YVO₄ crystals, respectively. The lasing thresholds for the lime operation can be seen to be nearly the same as the results obtained in the orange operation, as shown in Figure 6. In other words, the thresholds for the yellow and lime performances are wholly determined by the SRS process. At a pump power of 26 W, the output power of 4.8 W generated

from the Nd:GdVO₄ crystal for the 558-nm emission is clearly greater than 4.0 W from the Nd:YVO₄ crystal for the 559-nm emission.

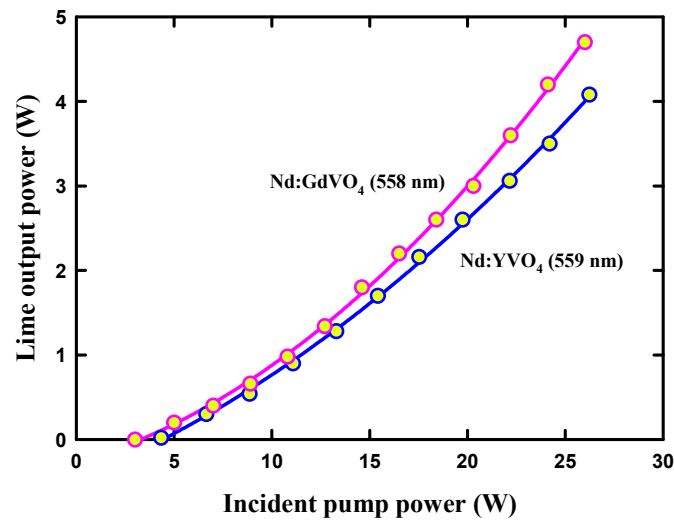


Figure 7. Average output powers versus the incident pump power for 558 and 559 nm obtained with the Nd:GdVO₄ and Nd:YVO₄ crystals, respectively.

When an LBO crystal ($\theta = 90^\circ, \phi = 11.6^\circ$) for the SHG phase matching of the fundamental field was exploited in the cavity, the green emission could be generated from the SHG of the fundamental wave. Figure 8 shows the average output powers versus the incident pump power for 531.5 and 532 nm generated from the Nd:GdVO₄ and Nd:YVO₄ crystals, respectively. Two pump thresholds are found to be almost the same, as low as 0.45 W. The output efficiency based on the Nd:GdVO₄ crystal is slightly lower than that based on Nd:YVO₄ crystal. The inferiority of the present Nd:GdVO₄ cavity for the SHG at 531.5 nm may come from the losses of the fundamental wave caused by the SRS process. In contrast, the influence of the SRS process on the SHG of the Nd:YVO₄ laser at 532 nm is relatively smaller due to a lower Raman gain.

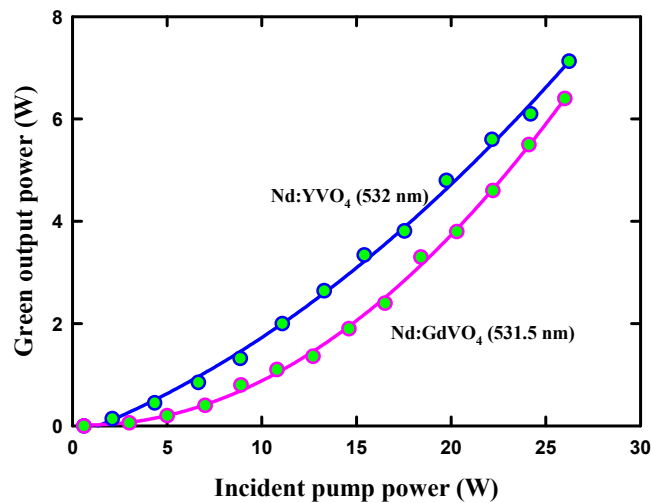


Figure 8. Average output powers versus the incident pump power for 531.5 and 532 nm generated from the Nd:GdVO₄ and Nd:YVO₄ crystals, respectively.

5. Dual-Wavelength Operations for Lime-Green and Orange-Green Emissions

5.1. Lime-Green Emission

Based on the Nd:YVO₄ self-Raman resonator for the 559 nm laser output, an additional LBO with the cutting angle at $\theta = 90^\circ$ and $\phi = 11.6^\circ$ was positioned behind the first LBO crystal for generating 532-nm output via the intracavity SHG of the fundamental wave [87]. Under this circumstance, the lime-green dual-wavelength operation can be efficiently achieved. Figure 9a shows the cavity setup for the lime-green dual-wavelength emission. The temperature of the first LBO crystal was kept at 25 °C for the optimal phase-matching of the lime emission, whereas the temperature of the second LBO crystal was flexibly changed within 14–29 °C for controlling the output power of the 532 nm emission. The SHG efficiency can be expressed as [96]

$$\eta = \frac{8\pi^2}{\lambda_1^2} \frac{1}{n_1^2 n_2} \frac{L^2}{\epsilon_0 c} d_{eff}^2 \left[\frac{\sin(\Delta k L / 2)}{(\Delta k L / 2)} \right]^2, \quad (13)$$

where Δk is the wave vector mismatch, λ_1 is the fundamental wavelength, n_1 is the fundamental refraction index, n_2 is the refraction index of the second harmonic wave, d_{eff} is the effective nonlinearity, L is the nonlinear crystal length, and ϵ_0 is the permittivity of free space. From Equation (13), the conversion efficiency of the SHG process achieves maximal for $\Delta k = 0$, whereas the efficiency will considerably decrease for $\Delta k L \neq 0$. The conversion efficiency is reduced to 1/2 of the maximum value for $\Delta k L = 2.784$. Therefore, the temperature bandwidth can be calculated with $\Delta T_{BW} = 2.784 / \gamma_T L$, where γ_T is given by

$$\gamma_T = \frac{4\pi}{\lambda_1} \left(\frac{\partial n_1}{\partial T} - \frac{\partial n_2}{\partial T} \right)_{T=T_{pm}}, \quad (14)$$

where T_{pm} is the temperature for the phase matching condition. From the LBO crystal length of $L = 8$ mm, the temperature bandwidth ΔT_{BW} could be calculated to be around 5.9 °C. For convenience, the temperature of the second LBO crystal is denoted as T_{532} . Figure 9b shows the 532 and 559 nm output powers and the total output power versus the temperature of the second LBO crystal T_{532} at the pump power of 31.6 W. The temperature bandwidth of the SHG at 532 nm was estimated to be around 6 °C from the experimental range of 17–23 °C. The experimental result is in good agreement with the theoretical calculation. When the temperature T_{532} was lowered from 29 °C to 23 °C, the 532 nm output power increased from 0.4 W to 4.3 W. Under this condition, the output power at 559 nm was found to be almost unchanged, with an average output power of approximately 4.2 W. In the dual-wavelength operation, the total output power can significantly increase from 4.8 W to 8.5 W for the temperature T_{532} , decreasing from 29 °C to 23 °C. Consequently, the overall conversion efficiency increases from 15.2% to 26.9% in the dual-wavelength operation. The green output could be up to the highest power of 7.5 W for the temperature T_{532} , decreasing from 23 °C to 20 °C. Under this circumstance, the lime output power was reduced from 4.2 W to 2.0 W. The dropping of the lime output power means that the generation of the 532 nm laser consumes too much of the fundamental wave, thereby affecting the conversion efficiency of the Raman laser. In other words, although the power of the Raman laser increases linearly with the 808 nm pump power, the multiple SHG and SFG processes may interfere with each other. Even so, the total conversion efficiency for the dual-wavelength emissions could reach 30.1% at $T_{532} = 20$ °C. The green output power displayed decreasing for the temperature T_{532} , decreasing from 20 °C to a lower value. The total output for the dual-wavelength emissions could achieve the maximal power of 10 W at $T_{532} = 18$ °C. Consequently, the conversion efficiency was up to 31.6%, and the green and lime output powers were 7.1 W and 2.9 W, respectively. When the temperature T_{532} was lower than 15 °C, the lime output power could return to 4.2 W.

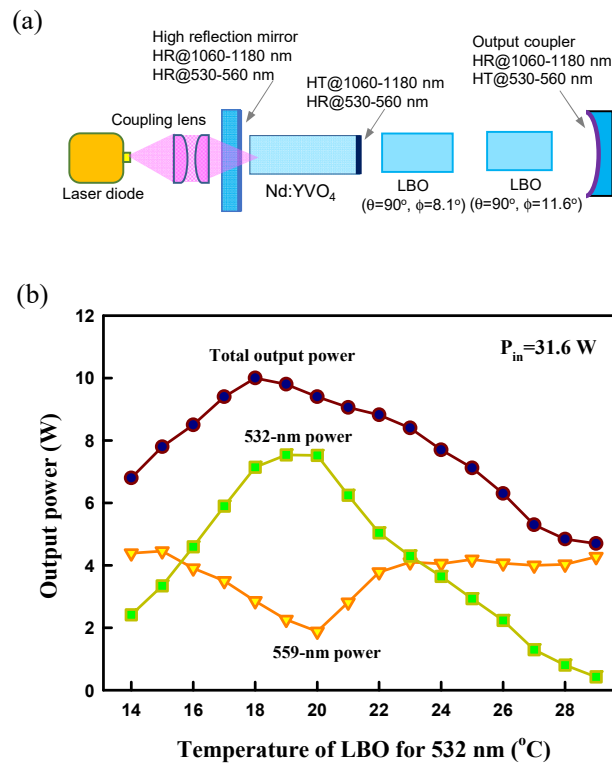


Figure 9. (a) Cavity configuration for the lime-green dual-wavelength operation. (b) Green and lime output powers and the total output power versus the temperature of the second LBO crystal T_{532} at the pump power of 31.6 W.

As shown in Figure 9b, the green and lime output powers are well balanced at $T_{532} = 23$ °C or 15.5 °C. For some applications of the dual-wavelength lasers, the balanced emissions are desirable and useful. Figure 10 shows the green and lime output powers and the total output power versus the pump power at $T_{532} = 23$ °C. The ratio of green and lime power was found to be within 1.1 ± 0.05 for the pump power in the range of 15.0–31.6 W. Experimental results revealed that the competition between the SFG and SHG was not conspicuous. The overall output variations for both wavelengths were generally smaller than $\pm 5\%$. Note that the order of the LBO crystals is critically important. Since the intensity of the Stokes wave is usually weaker than that of the fundamental wave, the SFG for the lime output should be performed in advance.

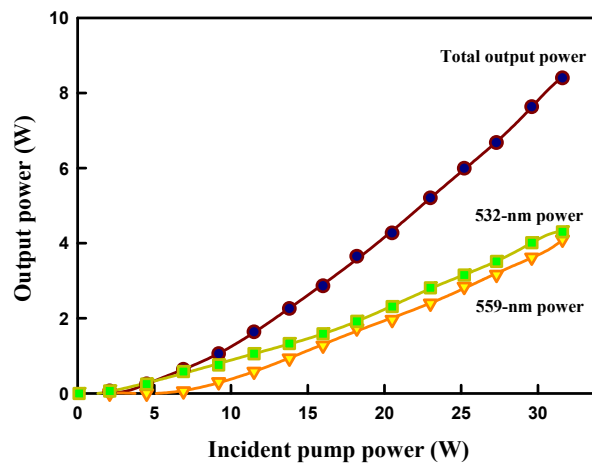


Figure 10. Green and lime output powers and the total output power versus the incident pump power at $T_{532} = 23$ °C.

In the experiment, the output spectra were measured with an optical spectrum analyzer (Advantest Q8381A) with a resolution of 0.1 nm. Figure 11 depicts the optical spectrum for the dual-wavelength emission at a pump power of 31.6 W at $T_{532} = 23\text{ }^{\circ}\text{C}$. The central wavelengths are around 532.5 and 559.1 nm. The spectral widths are approximately 0.4 and 0.2 nm for the green and lime outputs, respectively. The transverse patterns are also shown in the inset of Figure 11. The beam quality factors for overall results were found to be around 3.5–4.0.

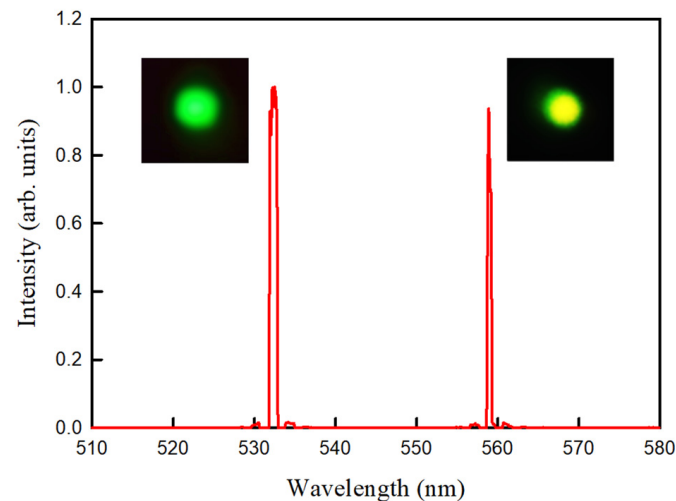


Figure 11. Optical spectrum for the dual-wavelength operation at a pump power of 31.6 W at $T_{532} = 23\text{ }^{\circ}\text{C}$.

5.2. Orange-Green Emission

In addition to the lime-green dual-wavelength emission, two LBO crystals could be exploited in the self-Raman laser cavity to generate the orange-green emission from the individual SHG of the Stokes and the fundamental waves [88]. Similar to the lime-green emission described above, the first LBO temperature was kept at the optimal phase-matching to obtain the maximum orange output power. Then, the second 8-mm-length LBO crystal with the cut angle at $\theta = 90^{\circ}$ and $\phi = 11.6^{\circ}$ was used to achieve the SHG of 1064 nm for green output power. As shown in Figure 9b, the optimal temperature of the second LBO crystal for the green generation was approximately $20\text{ }^{\circ}\text{C}$. The power ratio between the orange and green emissions could be flexibly adjusted by controlling the second LBO temperature to manipulate the SHG conversion efficiency for 532 nm. Figure 12 shows experimental results for the green, the orange, and the total output powers varying with the second LBO temperature at a pump power of 31.6 W. It can be seen that when the temperature changes from $28\text{ }^{\circ}\text{C}$ to $23\text{ }^{\circ}\text{C}$, the green output power increases from 0.2 W to 4.0 W, and the orange output power can be almost maintained at approximately 4.0 W. In other words, the total output power in the orange-green dual-wavelength operation can increase from 4.0 W to 8.0 W for the temperature of the second LBO crystal changing from $28\text{ }^{\circ}\text{C}$ to $23\text{ }^{\circ}\text{C}$, correspondingly, the overall conversion efficiency increasing from 12.7% to 25.4%. When the temperature of the second LBO crystal changes from $23\text{ }^{\circ}\text{C}$ to $19\text{ }^{\circ}\text{C}$, the green output power can be continually boosted up to the maximal value of 6.1 W. Under this circumstance, the orange output power at 588 nm can be seen to be reduced from 4.0 W to 2.2 W. Nevertheless, the total conversion efficiency at the temperature of $19\text{ }^{\circ}\text{C}$ in the dual-wavelength operation can achieve the highest value of 26.3% with the green and orange output powers to be 6.1 W and 2.2 W, respectively. When the temperature of the second LBO crystal starts to be lower than $19\text{ }^{\circ}\text{C}$, the green output power gradually decreases from the maximal value, and simultaneously, the orange emission returns to the power level of 4.0 W.

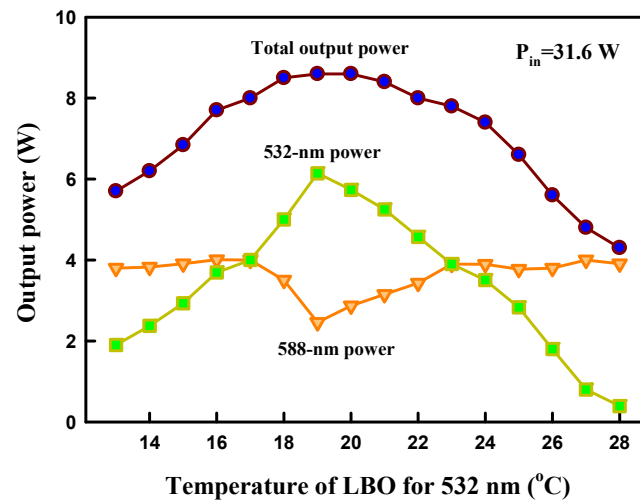


Figure 12. Experimental results for the green, the orange, and the total output powers vary with the temperature of the second LBO crystal at a pump power of 31.6 W.

Figure 13 shows the optical spectra at a pump power of 31.6 W for the orange-green dual-wavelength operation at four different temperatures of 19, 23, 26, and 28 °C for the second LBO crystal. The various ratios of the orange-green powers can be clearly seen in the lasing spectra. The transverse patterns of the total intensities are also shown in the insets of Figure 13. The colors of the transverse patterns can be found to vary from green-rich to orange-rich for the temperature of the second LBO crystal changing from 19 °C to 28 °C. The beam quality factors of both wavelengths were found to be approximately 3.5 at the maximal pump power of 31.6 W. As seen in Figure 12, the green and orange output powers can be almost balanced for the temperature of the second LBO crystal to be controlled at 23 °C or 17 °C. Figure 14 shows the green and orange output powers and the total output power versus the incident pump power at the temperature of 23 °C. The ratio of green to orange output powers can be found to be maintained at 1.0 ± 0.1 for the pump power within 10.0–31.6 W.

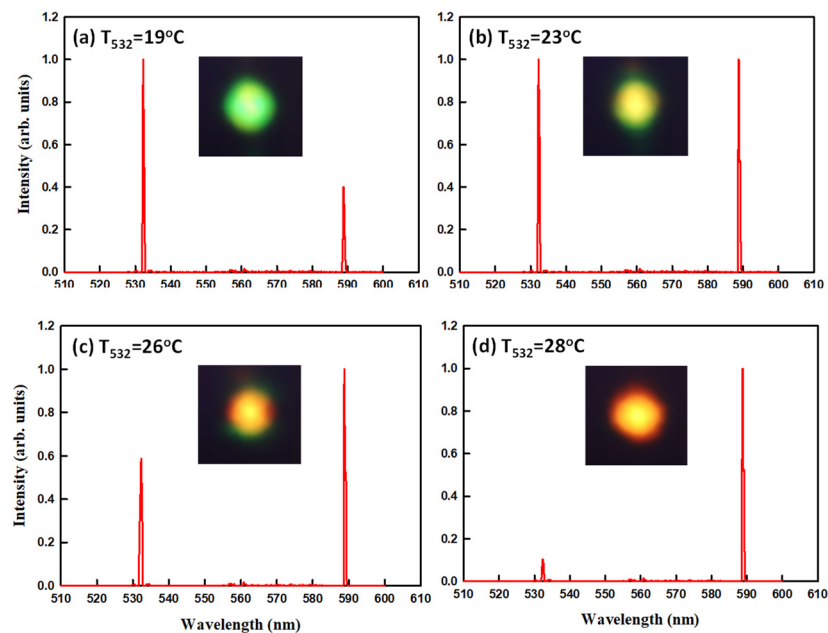


Figure 13. Optical spectra and transverse patterns at a pump power of 31.6 W for the orange-green operation at four different temperatures of 19, 23, 26, and 28 °C for the second LBO crystal.

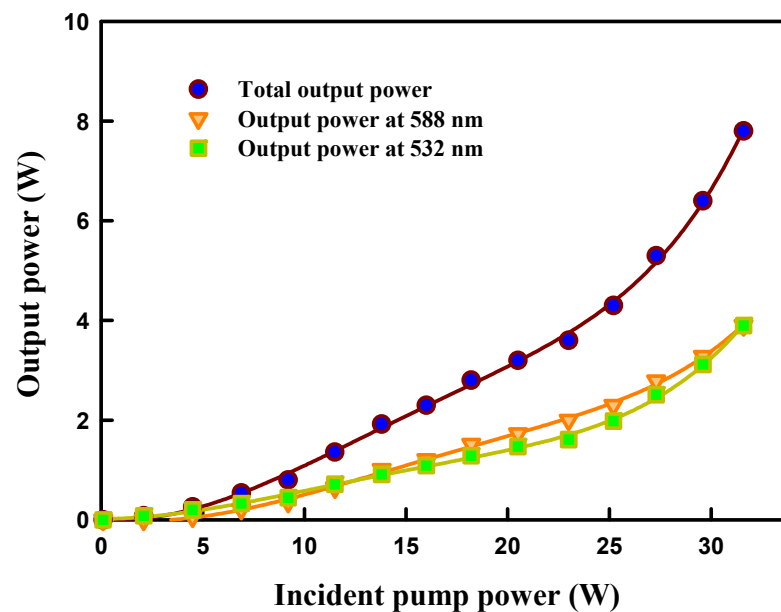


Figure 14. Green and orange output powers and the total output power versus the incident pump power at the temperature of 23 °C.

6. Triple-Wavelength Operation of Orange-Lime-Green Simultaneous Emissions

As reviewed in the previous section, the dual-wavelength operations of orange-green and lime-green emissions have been successfully implemented by using Nd:YVO₄ self-Raman lasers [87,88]. Furthermore, a reliable method for achieving the triple-wavelength operation with emissions of 588, 559, and 532 nm was also developed [89]. The developed method can provide the output powers of 588, 559, and 532 nm with a good balance. The method consists of three steps by using three LBO materials to generate the 588 nm, 559 nm and 532 nm lasers in sequence. The first step to set up the cavity is to maximize the 588 nm orange output by using the first LBO crystal, as discussed in the previous section.

The second step is to employ another LBO material to accomplish the dual-wavelength operation of orange-lime emissions at 588 and 559 nm, as shown in Figure 15a. The second LBO material was 8 mm in length, and the cutting angle was at $\theta = 90^\circ$ and $\phi = 8.1^\circ$ for the lime emission from the SFG of the fundamental and Stokes fields. The temperature of the first LBO crystal was fixed at 23.5 °C for the optimal orange emission. Under this condition, the output power ratio between the orange and lime emissions could be varied in a wide range by adjusting the temperature of the second LBO material. Figure 15b shows the lime and orange output powers versus the temperature of the second LBO crystal at a pump power of 30 W. The lime and orange output powers can be found to be well balanced for the temperature of the second LBO material at 20 °C or 27.5 °C. As shown in Figure 15b, both lime and orange output powers at the balanced temperature of 27.5 °C are nearly close to 2.6 W at the incident pump power of 30 W. Under the dual-wavelength orange-lime operation, the conversion efficiency is approximately 17.3%. Once again, the order of the LBO crystals is critically important. Since the intensity of the Stokes wave is usually weaker than that of the fundamental wave, the SHG for the orange output should be performed in advance. Figure 16 shows the orange and lime output powers versus the incident pump power at the balanced temperature of 27.5 °C. It can be seen that the orange and lime output powers can be well balanced for the pump power within 10–30 W.

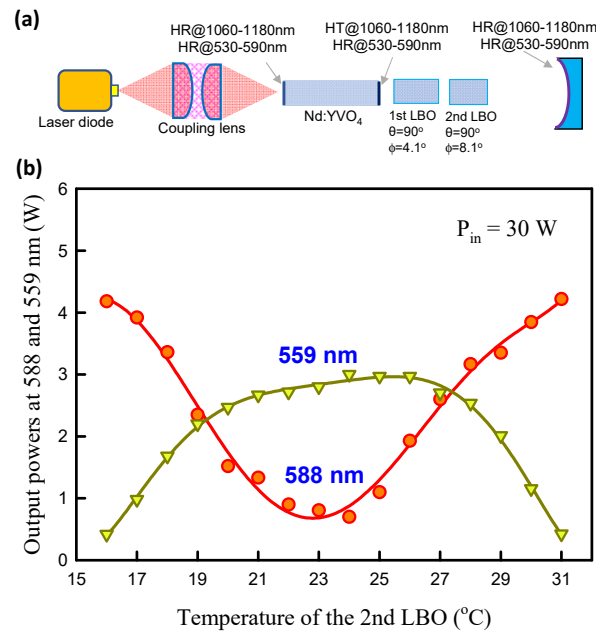


Figure 15. (a) Cavity setup for dual-wavelength output of orange-lime emissions at 588 and 559 nm. (b) Lime and orange output powers versus the second LBO temperature at a pump power of 30 W.

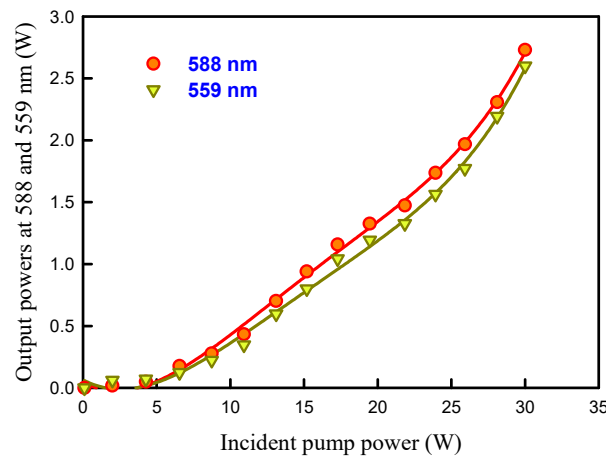


Figure 16. Orange and lime output powers versus pump power at a balanced temperature of 27.5 °C.

The final step for accomplishing the triple-wavelength operation is to exploit the third LBO material for generating the green output power in the laser cavity, as shown in Figure 17a. From the resonator setup shown in Figure 15a, the third LBO material was positioned behind the second LBO crystal. The length of the third LBO crystal was 8 mm and the cutting angle was at $\theta = 90^\circ$ and $\phi = 11.6^\circ$. By maintaining the first and second LBO crystals at the temperatures for the equal orange and lime emissions, the power ratio between the orange-lime and green outputs could be varied by controlling the temperature of the third LBO material in the range of 14–36 °C. Figure 17b shows the experimental results for the orange, lime, and green output powers versus the third LBO temperature at a pump power of 30 W. Experimental results revealed that the equal emissions for the orange and lime lasers were not significantly affected by adding the third LBO material into the resonator. The green output power at 532 nm could increase from 0.3 W to 2.4 W by changing the third LBO temperature from 36 °C to 27 °C. Under this condition, both the orange and lime output powers were found to be approximately 2.5 W without significant variation. By decreasing the third LBO temperature from 27 °C to 20 °C, the green output could continuously increase up to the highest power of 4.6 W. Under this circumstance,

both the orange and lime output powers were found to decrease from 2.5 W to 1.9 W. For the third LBO temperature at 20 °C, the total conversion efficiency in the triple-wavelength operation could reach 27% with the green, lime, and orange output powers to be 4.6 W, 1.9 W and 2.0 W, respectively. When the third LBO temperature was lower than 20 °C, the green output power turned to decrease. Under this condition, both the orange and lime output powers were progressively back to the power level of 2.5 W. For the third LBO temperature at 27 °C, the green, lime, and orange output powers could be nearly equal, as seen in Figure 17b. Figure 18 shows the green, lime, and orange output powers versus the pump power for the third LBO temperature at 27 °C. The power ratio of the three outputs could be approximately 1.0 ± 0.1 for the pump power within 10–30 W. To be brief, the equal output powers for the three wavelengths could be maintained for the pump power within 10–30 W.

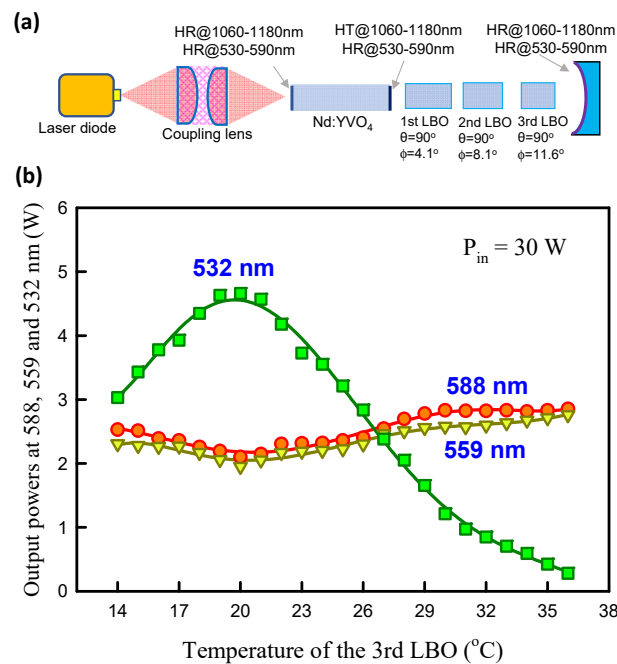


Figure 17. (a) Cavity setup for the triple-wavelength output for generating orange-lime-green emissions. (b) Experimental results for the orange, lime, and green output powers versus the third LBO temperature at a pump power of 30 W.

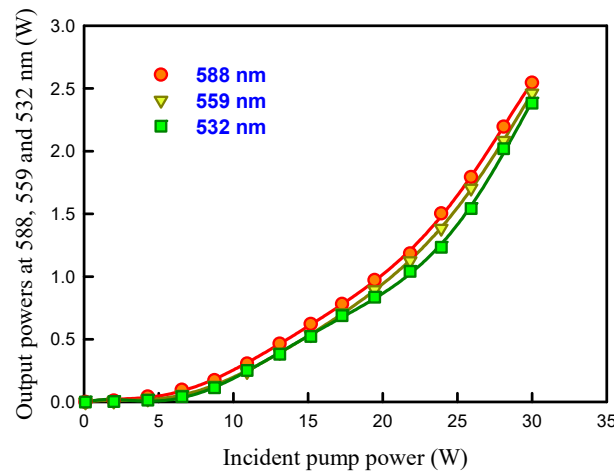


Figure 18. Green, lime, and orange output powers versus the incident pump power at the temperature of 27 °C.

Figure 19 shows the optical spectra and transverse patterns measured at the incident pump power of 30 W for the triple-wavelength operation for the third LBO crystal at four different temperatures of 20, 27, 29, and 36 °C. The various power ratios can be clearly seen from the optical spectra. The colors of the entire output beams exhibited the transformation from green-rich to orange-rich for the third LBO temperature varying from 20 °C to 36 °C. The overall beam quality factors for triple-wavelengths were measured to be around 3.0–4.0 at a pump power of 30 W.

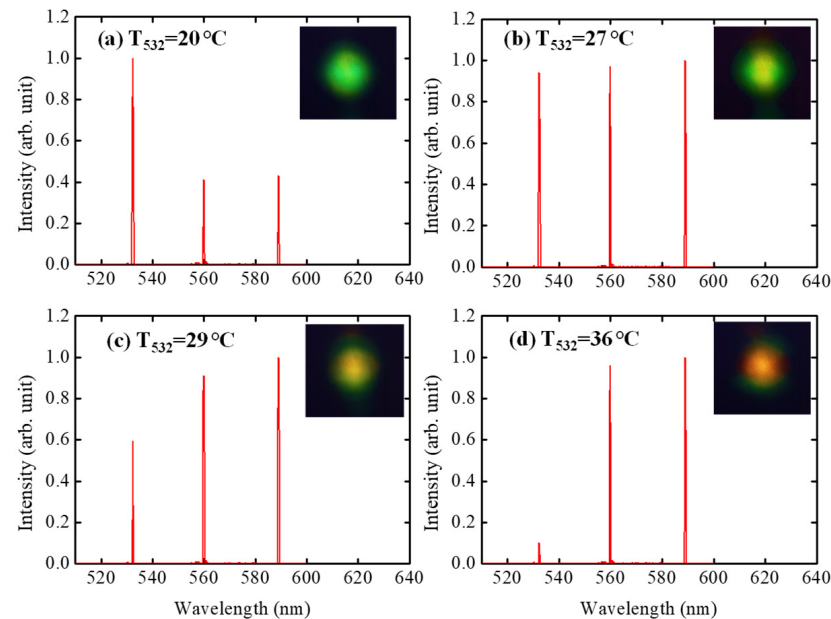


Figure 19. Optical spectra and transverse patterns measured at the incident pump power of 30 W for the triple-wavelength operation for the third LBO crystal at four different temperatures of 20, 27, 29, and 36 °C.

7. Conclusions

We have thoroughly reviewed the recent development of compact high-power CW orange-lime-green lasers by combining intracavity SRS in Nd-doped vanadate lasers with SFG and SHG in LBO crystals. We have overviewed the properties of the spontaneous Raman spectra in Nd:YVO₄ and Nd:GdVO₄ crystals, as well as the critical phase matchings of LBO crystal for visible emissions from SFG and SHG. The self-Raman lasers with vanadate and LBO crystals to achieve the individual green-lime-orange emissions have been systematically reviewed. We have presented a detailed review of the dual-wavelength operations of the lime-green and orange-green lasers. Finally, the procedure for generating the triple-wavelength operation of orange-lime-green simultaneous emissions has been discussed. The present review is expected to be of practical usefulness for designing compact, efficient, high-power CW visible lasers.

Author Contributions: Conceptualization, D.L. and Y.-F.C.; validation, X.-W.C. and C.-Y.H.; formal analysis, C.-Y.H. and H.-C.L.; resources, X.-W.C. and D.L.; writing—original draft preparation, Y.-F.C.; writing—review and editing, H.-C.L., D.L. and Y.-F.C.; supervision, Y.-F.C. All authors have read and agreed to the published version of the manuscript.

Funding: This work is supported by the National Science and Technology Council of Taiwan (contract number 112-2112-M-A49-022-MY3).

Institutional Review Board Statement: Not applicable.

Informed Consent Statement: Not applicable.

Data Availability Statement: Not applicable.

Conflicts of Interest: The authors declare no conflicts of interest.

References

- Karlin, D.B. *Lasers in Ophthalmic Surgery*; Blackwell Science: Cambridge, MA, USA, 1995; pp. 22–25.
- Desmettre, T.; Maurage, C.A.; Mordon, S. Transpupillary thermotherapy (TTT) with short duration laser exposures induce heat shock protein (HSP) hyperexpression on choroidretinal layers. *Laser Surg. Med.* **2003**, *33*, 102–107.
- Lock, J.H.; Fong, K.C. Retinal laser photocoagulation. *Med. J. Malays.* **2010**, *65*, 88–94.
- Lock, J.H.; Fong, K.C. An update on retinal laser therapy. *Clin. Exp. Optom.* **2011**, *94*, 43–51.
- Woodbury, E.; Ng, W. Ruby laser operation in near IR. *Proc. Inst. Radio. Eng.* **1962**, *50*, 2367.
- Ammann, E.O.; Falk, J. Stimulated Raman scattering at kHz pulse repetition rates. *Appl. Phys. Lett.* **1975**, *27*, 662–664.
- Basiev, T.T.; Powell, R.C. Solid-state Raman lasers. In *Handbook of Laser Technology and Applications*; Webb, C.E., Ed.; The Institute of Physics: London, UK; Bristol, UK, 2003.
- Cerný, P.; Jelinkova, H.; Zverev, P.G.; Basiev, T.T. Solid state lasers with Raman frequency conversion. *Prog. Quantum Electron.* **2004**, *28*, 113–143.
- Demidovich, A.; Grabtchikov, A.; Lisinetskii, V.; Burakevich, V.; Orlovich, V.; Kiefer, W. Continuous-wave Raman generation in a diode-pumped Nd³⁺:KGd(WO₄)₂ laser. *Opt. Lett.* **2005**, *30*, 1701–1703.
- Piper, J.A.; Pask, H.M. Crystalline Raman Lasers. *IEEE J. Sel. Top. Quantum Electron.* **2007**, *13*, 692–704.
- Dekker, P.; Pask, H.M.; Spence, D.J.; Piper, J.A. Continuous-wave, intracavity doubled, self-Raman laser operation in Nd:GdVO₄ at 586.5 nm. *Opt. Express* **2007**, *15*, 7038–7046. [[CrossRef](#)] [[PubMed](#)]
- Zhu, H.; Duan, Y.; Zhang, G.; Huang, C.; Wei, Y.; Chen, W.; Huang, Y.; Ye, N. Yellow-light generation of 5.7 W by intracavity doubling self-Raman laser of YVO₄/Nd:YVO₄ composite. *Opt. Lett.* **2009**, *34*, 2763–2765. [[CrossRef](#)] [[PubMed](#)]
- Lü, Y.; Cheng, W.; Xiong, Z.; Lu, J.; Xu, L.; Sun, G.; Zhao, Z. Efficient CW laser at 559 nm by intracavity sum-frequency mixing in a self-Raman Nd:YVO₄ laser under direct 880 nm diode laser pumping. *Laser Phys. Lett.* **2010**, *7*, 787. [[CrossRef](#)]
- Lee, A.J.; Spence, D.J.; Piper, J.A.; Pask, H.M. A wavelength-versatile, continuous-wave, self-Raman solid-state laser operating in the visible. *Opt. Express* **2010**, *18*, 20013–20018. [[CrossRef](#)] [[PubMed](#)]
- Kananovich, A.; Demidovich, A.; Danailov, M.; Grabtchikov, A.; Orlovich, V. All-solid-state quasi-CW yellow laser with intracavity self-Raman conversion and sum frequency generation. *Laser Phys. Lett.* **2010**, *7*, 573–578. [[CrossRef](#)]
- Lin, J.; Pask, H.M. Cascaded self-Raman lasers based on 382 cm⁻¹ shift in Nd:GdVO₄. *Opt. Express* **2012**, *20*, 15180–15185. [[CrossRef](#)] [[PubMed](#)]
- Andriunas, K.; Vishchakas, I.; Kabelka, V.; Mochalov, I.; Pavliuk, A. Stimulated-Raman self-conversion of Nd³⁺ laser light in double tungstenate crystals. *ZhETF Pisma Redaktsiiu* **1985**, *42*, 333–335.
- Grabtchikov, A.; Kuzmin, A.; Lisinetskii, V.; Orlovich, V.; Ryabtsev, G.; Demidovich, A. All solid-state diode-pumped Raman laser with self-frequency conversion. *Appl. Phys. Lett.* **1999**, *75*, 3742–3744. [[CrossRef](#)]
- Grabtchikov, A.; Kuzmin, A.; Lisinetskii, V.; Ryabtsev, G.; Orlovich, V.; Demidovich, A. Stimulated Raman scattering in Nd:KGW laser with diode pumping. *J. Alloy. Compd.* **2000**, *300*, 300–302. [[CrossRef](#)]
- Ustimenko, N.S.; Gulin, A.V. New self-frequency converted Nd³⁺:KGd(WO₄)₂ Raman lasers. *Quantum Electron.* **2002**, *32*, 229. [[CrossRef](#)]
- Omatsu, T.; Ojima, Y.; Pask, H.M.; Piper, J.A.; Dekker, P. Efficient 1181 nm self-stimulating Raman output from transversely diode-pumped Nd³⁺:KGd(WO₄)₂ laser. *Opt. Commun.* **2004**, *232*, 327–331. [[CrossRef](#)]
- Hamano, A.; Pleasants, S.; Okida, M.; Itoh, M.; Yatagai, T.; Watanabe, T.; Fujii, M.; Iketaki, Y.; Yamamoto, K.; Omatsu, T. Highly efficient 1181 nm output from a transversely diode-pumped Nd³⁺:KGd(WO₄)₂ self-stimulating Raman laser. *Opt. Commun.* **2006**, *260*, 675–679. [[CrossRef](#)]
- Jianhong, H.; Jipeng, L.; Rongbing, S.; Jinghui, L.; Hui, Z.; Canhua, X.; Fei, S.; Zongzhi, L.; Jian, Z.; Wenrong, Z. Short pulse eye-safe laser with a stimulated Raman scattering self-conversion based on a Nd:KGW crystal. *Opt. Lett.* **2007**, *32*, 1096–1098. [[CrossRef](#)] [[PubMed](#)]
- Lisinetskii, V.; Grabtchikov, A.; Demidovich, A.; Burakevich, V.; Orlovich, V.; Titov, A. Nd:KGW/KGW crystal: Efficient medium for continuous-wave intracavity Raman generation. *Appl. Phys. B* **2007**, *88*, 499–501. [[CrossRef](#)]
- Chunaev, D.; Basiev, T.; Konushkin, V.; Papashvili, A.; Karasik, A.Y. Synchronously pumped intracavity YLF–Nd–KGW picosecond Raman lasers and LiF:F⁻² amplifiers. *Laser Phys. Lett.* **2008**, *5*, 589–592. [[CrossRef](#)]
- Tang, C.Y.; Zhuang, W.Z.; Su, K.W.; Chen, Y.F. Efficient continuous-wave self-Raman Nd:KGW laser with intracavity cascade emission based on shift of 89 cm⁻¹. *IEEE J. Sel. Top. Quantum Electron.* **2014**, *21*, 142–147. [[CrossRef](#)]
- Kisel, V.; Shcherbitsky, V.; Kuleshov, N. Efficient self-frequency Raman conversion in a passively Q-switched diode-pumped Yb:KGd(WO₄)₂ laser. In Proceedings of the Advanced Solid-State Photonics, San Antonio, TX, USA, 2–5 February 2003; p. 189.
- Chang, M.T.; Zhuang, W.; Su, K.W.; Yu, Y.; Chen, Y.F. Efficient continuous-wave self-Raman Yb:KGW laser with a shift of 89 cm⁻¹. *Opt. Express* **2013**, *21*, 24590–24598. [[CrossRef](#)]
- Ferreira, M.S.; Wetter, N.U. Yb:KGW self-Raman laser with 89 cm⁻¹ Stokes shift and more than 32% diode-to-Stokes optical efficiency. *Opt. Laser Technol.* **2020**, *121*, 105835. [[CrossRef](#)]
- Chen, W.; Inagawa, Y.; Omatsu, T.; Tateda, M.; Takeuchi, N.; Usuki, Y. Diode-pumped, self-stimulating, passively Q-switched Nd³⁺:PbWO₄ Raman laser. *Opt. Commun.* **2001**, *194*, 401–407. [[CrossRef](#)]

31. Šulc, J.; Jeli, H.; Basiev, T.; Doroschenko, M.; Ivleva, L.; Osiko, V.; Zverev, P. Nd:SrWO₄ and Nd:BaWO₄ Raman lasers. *Opt. Mater.* **2007**, *30*, 195–197. [[CrossRef](#)]
32. Jelinkova, H.; Šulc, J.; Basiev, T.; Zverev, P.; Kravtsov, S. Stimulated Raman scattering in Nd:SrWO₄. *Laser Phys. Lett.* **2004**, *2*, 4. [[CrossRef](#)]
33. Liu, J.; Griebner, U.; Petrov, V.; Zhang, H.; Zhang, J.; Wang, J. Efficient continuous-wave and Q-switched operation of a diode-pumped Yb:KLu(WO₄)₂ laser with self-Raman conversion. *Opt. Lett.* **2005**, *30*, 2427–2429. [[CrossRef](#)]
34. Cong, Z.; Liu, Z.; Qin, Z.; Zhang, X.; Zhang, H.; Li, J.; Yu, H.; Wang, W. LD-pumped actively Q-switched Nd:KLu(WO₄)₂ self-Raman laser at 1185 nm. *Opt. Laser Technol.* **2015**, *73*, 50–53. [[CrossRef](#)]
35. Kaminskii, A.A.; Eichler, H.J.; Ueda, K.-i.; Klassen, N.V.; Redkin, B.S.; Li, L.E.; Findeisen, J.; Jaque, D.; Garcia-Sole, J.; Fernández, J. Properties of Nd³⁺-doped and undoped tetragonal PbWO₄, NaY(WO₄)₂, CaWO₄, and undoped monoclinic ZnWO₄ and CdWO₄ as laser-active and stimulated Raman scattering-active crystals. *Appl. Opt.* **1999**, *38*, 4533–4547. [[CrossRef](#)] [[PubMed](#)]
36. Chen, Y.F. Efficient 1521-nm Nd:GdVO₄ Raman laser. *Opt. Lett.* **2004**, *29*, 2632–2634. [[CrossRef](#)]
37. Su, F.; Zhang, X.; Wang, Q.; Jia, P.; Li, S.; Liu, B.; Zhang, X.; Cong, Z.; Wu, F. Theoretical and experimental study on a diode-pumped actively Q-switched Nd:GdVO₄ self-stimulated Raman laser at 1173 nm. *Opt. Commun.* **2007**, *277*, 379–384. [[CrossRef](#)]
38. Chen, Y.F. Compact efficient self-frequency Raman conversion in diode-pumped passively Q-switched Nd:GdVO₄ laser. *Appl. Phys. B* **2004**, *78*, 685–687. [[CrossRef](#)]
39. Basiev, T.; Vassiliev, S.; Konjushkin, V.; Osiko, V.; Zagumennyi, A.; Zavartsev, Y.; Kutovoi, S.; Shcherbakov, I. Diode pumped 500-picosecond Nd:GdVO₄ Raman laser. *Laser Phys. Lett.* **2004**, *1*, 237. [[CrossRef](#)]
40. Baoshan, W.; Huiming, T.; Jiying, P.; Jieguang, M.; Lanlan, G. Low threshold, diode end-pumped Nd³⁺:GdVO₄ self-Raman laser. *Opt. Mater.* **2007**, *29*, 1817–1820. [[CrossRef](#)]
41. Lee, A.; Pask, H.M.; Dekker, P.; Piper, J. High efficiency, multi-Watt CW yellow emission from an intracavity-doubled self-Raman laser using Nd:GdVO₄. *Opt. Express* **2008**, *16*, 21958–21963. [[CrossRef](#)]
42. Lee, A.J.; Pask, H.M.; Spence, D.J.; Piper, J.A. Efficient 5.3 W cw laser at 559 nm by intracavity frequency summation of fundamental and first-Stokes wavelengths in a self-Raman Nd:GdVO₄ laser. *Opt. Lett.* **2010**, *35*, 682–684. [[CrossRef](#)]
43. Lee, A.J.; Lin, J.; Pask, H.M. Near-infrared and orange-red emission from a continuous-wave, second-Stokes self-Raman Nd:GdVO₄ laser. *Opt. Lett.* **2010**, *35*, 3000–3002. [[CrossRef](#)]
44. Omatsu, T.; Okida, M.; Lee, A.; Pask, H. Thermal lensing in a diode-end-pumped continuous-wave self-Raman Nd-doped GdVO₄ laser. *Appl. Phys. B* **2012**, *108*, 73–79. [[CrossRef](#)]
45. Lin, J.; Pask, H. Nd:GdVO₄ self-Raman laser using double-end polarised pumping at 880 nm for high power infrared and visible output. *Appl. Phys. B* **2012**, *108*, 17–24. [[CrossRef](#)]
46. Wang, M.; Ding, S.; Yu, W.; Zhang, W. High-efficient diode-pumped passively Q-switched c-cut Nd:GdVO₄ self-Raman laser. *Laser Phys. Lett.* **2013**, *10*, 045403. [[CrossRef](#)]
47. Kang, P.; Zhang, X.; Jing, X.; Chen, C.; Pang, S.; Huang, J. Dual-wavelength passively Q-switched Ho:GdVO₄ self-Raman laser operating at 2473 nm and 2520 nm. *Opt. Lett.* **2023**, *48*, 3495–3498. [[CrossRef](#)] [[PubMed](#)]
48. Ma, Y.; Sugahara, H.; Lee, A.J.; Pask, H.M.; Miyamoto, K.; Omatsu, T. Watt-Level 1173 nm Laguerre-Gaussian Mode Generation From a Self-Raman Nd:GdVO₄ Laser. *J. Lightwave Technol.* **2023**, *41*, 2087–2093. [[CrossRef](#)]
49. She, K.; Zhou, P.; Wei, Y.; Xu, S.; Li, B.; Liao, W.; Lin, Z.; Zhang, G. Manipulation of linearly polarized states in a c-cut Nd:YVO₄ passively Q-switched self-Raman laser. *Appl. Phys. B* **2024**, *130*, 51. [[CrossRef](#)]
50. Chen, Y.F. High-power diode-pumped actively Q-switched Nd:YVO₄ self-Raman laser: Influence of dopant concentration. *Opt. Lett.* **2004**, *29*, 1915–1917. [[CrossRef](#)]
51. Chen, Y.F. Compact efficient all-solid-state eye-safe laser with self-frequency Raman conversion in a Nd:YVO₄ crystal. *Opt. Lett.* **2004**, *29*, 2172–2174. [[CrossRef](#)]
52. Fan, L.; Zhao, W.; Qiao, X.; Xia, C.; Wang, L.; Fan, H.; Shen, M. An efficient continuous-wave YVO₄/Nd:YVO₄/YVO₄ self-Raman laser pumped by a wavelength-locked 878.9 nm laser diode. *Chin. Phys. B* **2016**, *25*, 114207. [[CrossRef](#)]
53. Chen, Y.F.; Chen, K.; Liu, Y.; Chen, C.; Tsou, C.; Liang, H. Criterion for optimizing high-power acousto-optically Q-switched self-Raman yellow lasers with repetition rates up to 500 kHz. *Opt. Lett.* **2020**, *45*, 1922–1925. [[CrossRef](#)]
54. Ding, S.; Zhang, X.; Wang, Q.; Su, F.; Jia, P.; Li, S.; Fan, S.; Chang, J.; Zhang, S.; Liu, Z. Theoretical and experimental study on the self-Raman laser with Nd:YVO₄ crystal. *IEEE J. Quantum Electron.* **2006**, *42*, 927–933. [[CrossRef](#)]
55. Chen, Y.F. Efficient subnanosecond diode-pumped passively Q-switched Nd:YVO₄ self-stimulated Raman laser. *Opt. Lett.* **2004**, *29*, 1251–1253. [[CrossRef](#)] [[PubMed](#)]
56. Su, F.; Zhang, X.; Wang, Q.; Ding, S.; Jia, P.; Li, S.; Fan, S.; Zhang, C.; Liu, B. Diode pumped actively Q-switched Nd:YVO₄ self-Raman laser. *J. Phys. D Appl. Phys.* **2006**, *39*, 2090. [[CrossRef](#)]
57. Wang, B.; Tan, H.; Peng, J.; Miao, J.; Gao, L. Low threshold, actively Q-switched Nd³⁺:YVO₄ self-Raman laser and frequency doubled 588 nm yellow laser. *Opt. Commun.* **2007**, *271*, 555–558. [[CrossRef](#)]
58. Burakevich, V.; Lisinetskii, V.; Grabtchikov, A.; Demidovich, A.; Orlovich, V.; Matrosov, V. Diode-pumped continuous-wave Nd:YVO₄ laser with self-frequency Raman conversion. *Appl. Phys. B* **2007**, *86*, 511–514. [[CrossRef](#)]
59. Lee, A.; Pask, H.; Omatsu, T.; Dekker, P.; Piper, J. All-solid-state continuous-wave yellow laser based on intracavity frequency doubled self-Raman laser action. *Appl. Phys. B* **2007**, *88*, 539–544. [[CrossRef](#)]

60. Weitz, M.; Theobald, C.; Wallenstein, R.; L’huillier, J.A. Passively mode-locked picosecond Nd:YVO₄ self-Raman laser. *Appl. Phys. Lett.* **2008**, *92*, 091122. [[CrossRef](#)]
61. Chen, X.; Zhang, X.; Wang, Q.; Li, P.; Cong, Z. Diode-pumped actively Q-switched c-cut Nd:YVO₄ self-Raman laser. *Laser Phys. Lett.* **2008**, *6*, 26. [[CrossRef](#)]
62. Chang, Y.T.; Su, K.W.; Chang, H.; Chen, Y.F. Compact efficient Q-switched eye-safe laser at 1525 nm with a double-end diffusion bonded Nd:YVO₄ crystal as a self-Raman medium. *Opt. Express* **2009**, *17*, 4330–4335. [[CrossRef](#)]
63. Omatsu, T.; Lee, A.; Pask, H.; Piper, J. Passively Q-switched yellow laser formed by a self-Raman composite Nd:YVO₄/YVO₄ crystal. *Appl. Phys. B* **2009**, *97*, 799–804. [[CrossRef](#)]
64. Zhu, H.; Duan, Y.; Zhang, G.; Huang, C.; Wei, Y.; Shen, H.; Zheng, Y.; Huang, L.; Chen, Z. Efficient second harmonic generation of double-end diffusion-bonded Nd:YVO₄ self-Raman laser producing 7.9 W yellow light. *Opt. Express* **2009**, *17*, 21544–21550. [[CrossRef](#)] [[PubMed](#)]
65. Wang, Z.; Du, C.; Ruan, S.; Zhang, L. LD-pumped Q-switched Nd:YVO₄ self-Raman laser. *Laser Phys.* **2010**, *20*, 474–477. [[CrossRef](#)]
66. Du, C.L.; Zhang, L.; Yu, Y.Q.; Ruan, S.; Guo, Y. 3.1 W laser-diode-end-pumped composite Nd:YVO₄ self-Raman laser at 1176 nm. *Appl. Phys. B* **2010**, *101*, 743–746. [[CrossRef](#)]
67. Zhu, H.; Duan, Y.; Zhang, G.; Huang, C.; Wei, Y.; Chen, W.; Huang, L.; Huang, Y. Efficient continuous-wave YVO₄/Nd:YVO₄ Raman laser at 1176 nm. *Appl. Phys. B* **2011**, *103*, 559–562. [[CrossRef](#)]
68. Fan, L.; Fan, Y.-X.; Wang, H.-T. A compact efficient continuous-wave self-frequency Raman laser with a composite YVO₄/Nd:YVO₄/YVO₄ crystal. *Appl. Phys. B* **2010**, *101*, 493–496. [[CrossRef](#)]
69. Fan, S.; Zhang, X.; Wang, Q.; Liu, Z.; Li, L.; Cong, Z.; Chen, X.; Zhang, X. 1097 nm Nd:YVO₄ self-Raman laser. *Opt. Commun.* **2011**, *284*, 1642–1644.
70. Li, X.; Lee, A.J.; Pask, H.M.; Piper, J.A.; Huo, Y. Efficient, miniature, cw yellow source based on an intracavity frequency-doubled Nd:YVO₄ self-Raman laser. *Opt. Lett.* **2011**, *36*, 1428–1430. [[CrossRef](#)] [[PubMed](#)]
71. Duan, Y.; Zhu, H.; Huang, C.; Zhang, G.; Wei, Y. Potential sodium D2 resonance radiation generated by intra-cavity SHG of a c-cut Nd:YVO₄ self-Raman laser. *Opt. Express* **2011**, *19*, 6333–6338. [[CrossRef](#)] [[PubMed](#)]
72. Duan, Y.; Zhang, G.; Zhang, Y.; Jin, Q.; Wang, H.; Zhu, H. LD end-pumped c-cut Nd:YVO₄/KTP self-Raman laser at 560 nm. *Laser Phys.* **2011**, *21*, 1859–1862. [[CrossRef](#)]
73. Chen, X.; Zhang, X.; Wang, Q.; Li, P.; Liu, Z.; Cong, Z.; Li, L.; Zhang, H. Highly efficient double-ended diffusion-bonded Nd:YVO₄ 1525-nm eye-safe Raman laser under direct 880-nm pumping. *Appl. Phys. B* **2012**, *106*, 653–656. [[CrossRef](#)]
74. Chen, W.; Wei, Y.; Huang, C.; Wang, X.; Shen, H.; Zhai, S.; Xu, S.; Li, B.; Chen, Z.; Zhang, G. Second-Stokes YVO₄/Nd:YVO₄/YVO₄ self-frequency Raman laser. *Opt. Lett.* **2012**, *37*, 1968–1970. [[CrossRef](#)] [[PubMed](#)]
75. Shen, H.; Wang, Q.; Zhang, X.; Liu, Z.; Bai, F.; Cong, Z.; Chen, X.; Wu, Z.; Wang, W.; Gao, L. Simultaneous dual-wavelength operation of Nd:YVO₄ self-Raman laser at 1524 nm and undoped GdVO₄ Raman laser at 1522 nm. *Opt. Lett.* **2012**, *37*, 4113–4115. [[CrossRef](#)] [[PubMed](#)]
76. Ding, S.; Wang, M.; Wang, S.; Zhang, W. Investigation on LD end-pumped passively Q-switched c-cut Nd:YVO₄ self-Raman laser. *Opt. Express* **2013**, *21*, 13052–13061. [[CrossRef](#)]
77. Huang, G.; Yu, Y.; Xie, X.; Zhang, Y.; Du, C. Diode-pumped simultaneously Q-switched and mode-locked YVO₄/Nd:YVO₄/YVO₄ crystal self-Raman first-Stokes laser. *Opt. Express* **2013**, *21*, 19723–19731. [[CrossRef](#)]
78. Du, C.; Huang, G.; Yu, Y.; Xie, X.; Zhang, Y.; Wang, D. Q-switched mode-locking of second-Stokes pulses in a diode-pumped YVO₄/Nd:YVO₄/YVO₄ self-Raman laser. *Laser Phys.* **2014**, *24*, 125003. [[CrossRef](#)]
79. Ding, X.; Fan, C.; Sheng, Q.; Li, B.; Yu, X.; Zhang, G.; Sun, B.; Wu, L.; Zhang, H.; Liu, J. 5.2-W high-repetition-rate eye-safe laser at 1525 nm generated by Nd:YVO₄–YVO₄ stimulated Raman conversion. *Opt. Express* **2014**, *22*, 29111–29116. [[CrossRef](#)]
80. Kores, C.C.; Jakutis-Neto, J.; Geskus, D.; Pask, H.M.; Wetter, N.U. Diode-side-pumped continuous wave Nd³⁺:YVO₄ self-Raman laser at 1176 nm. *Opt. Lett.* **2015**, *40*, 3524–3527. [[CrossRef](#)] [[PubMed](#)]
81. Lin, H.; Huang, X.; Sun, D.; Liu, X. Passively Q-switched multi-wavelength Nd:YVO₄ self-Raman laser. *J. Mod. Opt.* **2016**, *63*, 2235–2237. [[CrossRef](#)]
82. Zhu, H.; Guo, J.; Ruan, X.; Xu, C.; Duan, Y.; Zhang, Y.; Tang, D. Cascaded self-Raman laser emitting around 1.2–1.3 μm based on a c-cut Nd:YVO₄ crystal. *IEEE Photonics J.* **2017**, *9*, 1–7.
83. Zhu, H.; Guo, J.; Duan, Y.; Zhang, J.; Zhang, Y.; Xu, C.; Wang, H.; Fan, D. Efficient 1.7 μm light source based on KTA-OPO derived by Nd:YVO₄ self-Raman laser. *Opt. Lett.* **2018**, *43*, 345–348. [[CrossRef](#)]
84. Bai, F.; Jiao, Z.; Xu, X.; Wang, Q. High power Stokes generation based on a secondary Raman shift of 259 cm⁻¹ of Nd:YVO₄ self-Raman crystal. *Opt. Laser Technol.* **2019**, *109*, 55–60. [[CrossRef](#)]
85. Chen, M.; Dai, S.; Zhu, S.; Yin, H.; Li, Z.; Chen, Z. Multi-watt passively Q-switched self-Raman laser based on a c-cut Nd:YVO₄ composite crystal. *JOSA B* **2019**, *36*, 524–532. [[CrossRef](#)]
86. Chen, Y.F.; Pan, Y.Y.; Liu, Y.C.; Cheng, H.P.; Tsou, C.H.; Liang, H.C. Efficient high-power continuous-wave lasers at green-lime-yellow wavelengths by using a Nd:YVO₄ self-Raman crystal. *Opt. Express* **2019**, *27*, 2029–2035. [[CrossRef](#)] [[PubMed](#)]
87. Chen, Y.F.; Liu, Y.C.; Gu, D.Y.; Pan, Y.Y.; Cheng, H.P.; Tsou, C.H.; Liang, H.C. High-power dual-color yellow–green solid-state self-Raman laser. *Laser Phys.* **2019**, *29*, 075802. [[CrossRef](#)]
88. Chen, Y.F.; Liu, Y.C.; Pan, Y.Y.; Gu, D.Y.; Cheng, H.P.; Tsou, C.H.; Liang, H.C. Efficient high-power dual-wavelength lime-green Nd:YVO₄ lasers. *Opt. Lett.* **2019**, *44*, 1323–1326. [[CrossRef](#)] [[PubMed](#)]

89. Liu, Y.C.; Chen, C.; Hsiao, J.C.; Pan, Y.Y.; Tsou, C.H.; Liang, H.C.; Chen, Y.F. Compact efficient high-power triple-color Nd:YVO₄ yellow-lime-green self-Raman lasers. *Opt. Lett.* **2020**, *45*, 1144–1147. [[CrossRef](#)] [[PubMed](#)]
90. Liu, P.; Qi, F.; Li, W.; Liu, Z.; Wang, Y.; Ding, X.; Yao, J. Self-Raman Nd-doped vanadate laser: A pump source of organic crystal based difference frequency generation. *J. Mod. Opt.* **2020**, *67*, 914–919. [[CrossRef](#)]
91. Chen, M.; Dai, S.; Yin, H.; Zhu, S.; Li, Z.; Chen, Z. Passively Q-switched yellow laser at 589 nm by intracavity frequency-doubled c-cut composite Nd:YVO₄ self-Raman laser. *Optics Laser Technol.* **2021**, *133*, 106534. [[CrossRef](#)]
92. Kaminskii, A.; Bettinelli, M.; Dong, J.; Jaque, D.; Ueda, K. Nanosecond Nd³⁺:LuVO₄ self-Raman laser. *Laser Phys. Lett.* **2009**, *6*, 374. [[CrossRef](#)]
93. Lü, Y.; Zhang, X.; Li, S.; Xia, J.; Cheng, W.; Xiong, Z. All-solid-state cw sodium D2 resonance radiation based on intracavity frequency-doubled self-Raman laser operation in double-end diffusion-bonded Nd³⁺:LuVO₄ crystal. *Opt. Lett.* **2010**, *35*, 2964–2966. [[CrossRef](#)]
94. Ferraro, J.R.; Nakamoto, K.; Brown, C.W. *Introductory Raman Spectroscopy*, 2nd ed.; Elsevier Inc.: Amsterdam, The Netherlands, 2003; ISBN 9780122541056.
95. Kaminskii, A.A.; Ueda, K.-I.; Eichler, H.J.; Kuwano, Y.; Kouta, H.; Bagaev, S.N.; Chyba, T.H.; Barnes, J.C.; Gad, G.M.; Murai, T. Tetragonal vanadates YVO₄ and GdVO₄—new efficient $\chi(3)$ -materials for Raman lasers. *Opt. Commun.* **2001**, *194*, 201–206. [[CrossRef](#)]
96. Nikogosyan, D.N. *Nonlinear Optical Crystals: A Complete Survey*; Springer: Berlin, Germany, 2005.
97. Velsko, S.P.; Webb, M.; Davis, L.; Huang, C. Phase matched harmonic generation in lithium triborate (LBO). *IEEE J. Quantum Electron.* **1991**, *27*, 2182–2192. [[CrossRef](#)]
98. Tang, Y.; Cui, Y.; Dunn, M.H. Thermal dependence of the principal refractive indices of lithium triborate. *J. Opt. Soc. Am. B* **1995**, *12*, 638–643. [[CrossRef](#)]

Disclaimer/Publisher’s Note: The statements, opinions and data contained in all publications are solely those of the individual author(s) and contributor(s) and not of MDPI and/or the editor(s). MDPI and/or the editor(s) disclaim responsibility for any injury to people or property resulting from any ideas, methods, instructions or products referred to in the content.